Accepted for publication in *Journal of Geophysical Research-Oceans, VOL. 103, NO. C2, Pages 3033-3040, February 15, 1998*.

A BASIN-SCALE OCEANIC INSTABILITY EVENT IN THE GULF OF ALASKA

Richard E. Thomson and James F. R. Gower

Institute of Ocean Sciences, Sidney, British Columbia, Canada

Abstract. A composite NOAA 14 satellite AVHRR (Advanced Very High Resolution Radiometer) image of the Gulf of Alaska for early March 1995 reveals a sequence of six anticyclonic oceanic eddies spanning more than 1500 km of the continental margin of North America from central British Columbia to central Alaska. Although isolated mesoscale eddies have previously been documented for this eastern boundary region, the composite image provides the first evidence that trains of such eddies can develop "simultaneously" along the entire coast. The 80 km radius and 250 km spacing of these warm-core eddies are consistent with a baroclinic instability event in the poleward coastal current that prevails along the northwest continental margin of North America in “winter” (roughly October through March). Wind data from offshore meteorological buoys, combined with partial cloud-free thermal images for January and February, suggest that the event was triggered in mid January by an abrupt, coast-wide reversal in the prevailing poleward wind. The instability event disrupted the alongshore transport of relatively warm, high salinity water and presumably resulted in a greatly enhanced cross-shore flux of brackish, nutrient-rich coastal water into the open ocean. Based on its basin-scale extent and more than two month duration, it is feasible that the event had a major impact on the early spring recruitment and survival of zooplankton and pelagic fish within the highly productive fishery zones of coastal British Columbia and Alaska. Less extensive eddy sequences found in several earlier satellite images for the region suggest that these instability events are fairly common. If so, this indicates that the poleward current that forms over the eastern Pacific continental slope in late fall (herein, the “Northeast Pacific Coastal Current”) is marginally stable and likely to deform into a series of mesoscale eddies following abrupt, basin-scale reversals in the seasonally dominant wind. Provided these wind events occur early enough in the season, the coastal current could reform with the onset of poleward winter winds.

1. Introduction

Coastal currents along the eastern continental margin of the Gulf of Alaska undergo marked seasonal variations associated with seasonal changes in the prevailing longshore wind and pressure gradient [*Strub et al.*, 1987; *Hickey*, 1989]. From the Columbia River northward, the coastal current system is further influenced by the large volume of brackish water entering the ocean from rivers, fjords and straits [*LeBlond et al.*, 1983]. Strong (~0.3 m/s), year-round, poleward-flowing buoyancy-driven currents are particularly well defined over the inner continental shelves of Vancouver Island [*LeBlond et al.*, 1986; *Thomson et al.*, 1989] and the Alaska Panhandle [*Royer*, 1981]. These low density flows, known separately as the Vancouver Island Coastal Current and the Alaska Coastal Current, are weakly coupled dynamically to flow over the outer shelf and slope.

During summer months, surface currents over the continental slope of British Columbia and Washington State are predominantly equatorward in response to the prevailing winds. Currents off the southeast coast of Alaska at this time are mainly poleward as part of the large-scale cyclonic circulation in the Gulf of Alaska. In winter, surface currents over the continental slope are predominantly poleward throughout the entire region, driven by moderate-to-strong southerly winds associated with the Aleutian low pressure regime [*Marmer*, 1926; *Thomson et al.*, 1989; *Hickey*, 1989; *Thomson and Ware*, 1996]. These surface-intensified winter currents, identified as the Alaska Current off southeast Alaska [*Dodimead et al.*, 1963; *Tabata*, 1975], the Haida Current off central British Columbia [*Thomson and Emery*, 1986], and the Davidson Current from northern California to southern British Columbia [*Hickey*, 1989], extend to central Alaska (near Kodiak Island) where the flow merges with the Alaskan Stream western boundary current [*Reed and Stabeno*, 1989]. Excluding the buoyancy-driven currents over the inner shelf, this extensive coastal current system (which we suggest calling the “Northeast Pacific Coastal Current”) is responsible for transporting relatively warm, high-salinity water poleward in winter over a major segment of the North America continental margin.

In this paper, we use satellite thermal imagery collected in the Gulf of Alaska in the spring of 1995 to show that the Northeast Pacific Coastal Current can deform into an extensive series of regularly-spaced mesoscale eddies. Formation of the eddies in early 1995 occurred almost simultaneously along a 1500 km segment of the coast and appears to have been triggered by an abrupt reversal in the coastal winds during a period of strong outflow winds from the continental interior. Several possible impacts of this event on the oceanography of the region are discussed.

2. Thermal imagery

To generate the composite thermal image in Plate 1, we combined raw advanced very high resolution radiometer (AVHRR) image data from the early afternoon passes of the NOAA 14 satellite for March 1, 2, 3 and 10, 1995. The relation between the raw signal values and sea surface temperature was then determined using simultaneous buoy observations. Large-scale gradients in pixel values were then subtracted from the composite to produce the contrast-stretched, pseudo-color image in Plate 1.

Table 1. *Satellite Number, Pass Number, and Times for the National Oceanic and Atmospheric Administration (NOAA) sea surface temperature images used in this study.*

NOAA Satellite	Pass No.	Date (1995)	Time (UTC)	Cloud-free Coastal Area
9	51874	January 4	1833	Northern British Columbia-southern Alaska
14	330	January 22	2047	British Columbia
9	52142	January 23	1929	Northern British Columbia-southern Alaska
14	344	January 23	2036	Northern British Columbia-southern Alaska
14	471	February 1	2040	Central Alaska
14	514	February 4	2148	South-central British Columbia
9	52424	February 12	1831	North British Columbia-SE Alaska
14	655	February 14	2142	Southeast Alaska
9	52481	February 16	1919	Southeast Alaska
14	867	March 1	2221	British Columbia
14	881	March 2	2211	Washington/Vancouver Island
14	895	March 3	2200	Alaskan Panhandle
14	994	March 10	2225	Alaska south coast (Kodiak area)

The last column gives the region of the image that was free of cloud. The last four images were used to construct Plate 1. Mesoscale eddies appear off northern British Columbia and southern Alaska in the images for February 12 onward but not in the earlier images.

Each of the four original satellite images was cloud-covered except for those portions of the Gulf of Alaska coast which were blanketed by clear Arctic air from the continental interior (Table 1). The first three images captured different cloud-free coastal regions from northern Washington State to Kodiak Island (central

Alaska) while the image for March 10 captured the region from Kodiak Island westward. The composite image is geometrically corrected, with pixels evenly spaced in latitude and longitude. Pixels have equal east-west and north-south separations of 1.5 km at the center of the image (54° N, 141° W). There are 1001 lines in the composite, each with 1628 pixels.

Each pixel in the composite thermal image represents the highest measured thermal radiance (lowest raw signal value) measured at the location of that pixel on the 4 combined days. Because cloud is almost always colder than the ocean, this method typically selects cloud-free pixels, except where a pixel is cloud covered in all four images. Using this selection criterion, a composite image was created for AVHRR band 4 (thermal image of surface temperature) and also for band 2 (near-infrared, showing visible features in which land and cloud appear bright). Brighter pixels in the band 2 composite indicated the presence of cloud in the composite data and were used to mask the band 4 composite whenever a threshold in band 2 was exceeded. Favorable illumination and atmospheric conditions allowed a clean composite to be formed from these images using this method. Cloud-free areas had sun elevations of 30°-50°, giving good illumination with no apparent glint. Atmospheric radiance in the cloud-free areas was sufficiently equal on all four days that edges of the well-defined cloud-free areas are not apparent in Plate 1.

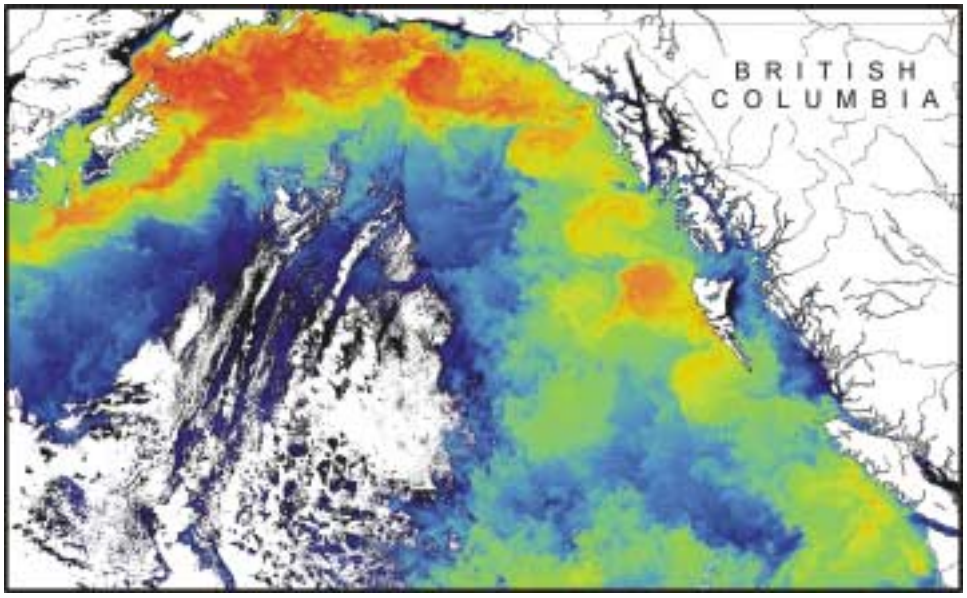

Plate 1. *A composite thermal (sea surface temperature) image for the Gulf of Alaska following removal of the average north-south temperature gradient. Oceanic temperatures differed from the mean north-south gradient by -3 C° (dark blue) to +3 C° (red). Clouds and land are white. Image is derived from NOAA 14 satellite Advanced Very High Resolution Radiometer (AVHRR) data for ~ 2200 UTC on March 1, 2, 3 and 10, 1995. The coastline and rivers have been added. Dotted line is the 1000 m depth contour.*

Water temperatures for digital pixel values in the resulting composite were determined using hourly sea surface temperatures provided by an array of meteorological buoys (Figure 1) for the times nearest those of the satellite passes. With the exception of buoy 46036 ("South Nomad"), temperatures derived from buoys in exposed oceanic locations agreed closely with a mean linear relation, with typical root-mean-square (rms) deviations of ~ 0.3 C°. A relatively high (1 C°) deviation for South Nomad can be explained by the occurrence of a large surface temperature gradient in the region. If the actual position of the buoy were ~ 5 km further north than the nominal position, the difference between the buoy sensor and satellite imager would be ~ 0.3 C°, similar to that for the other buoys. We use the mean relation derived from these “exposed” buoys when interpreting signal levels in terms of seas surface temperatures. Buoys in the more sheltered coastal waters, to the east of the eddy region discussed in this paper, showed higher scatter and a different mean relation with buoy temperatures, corresponding to lower measured satellite radiances. We interpret this as the effect of the cold air mass which was responsible for the clear atmospheric conditions of the March satellite observations.

The thermal contrasts, which make the eddies visible in Plate 1, correspond to a small signal range equal to ~ 30 levels of digitization in the AVHRR raw data. The original form of the composite image showed a strong north-south temperature gradient, of ~ 30 levels across the area shown, and an apparent lowering in water

temperature towards the western edge due to increased atmospheric absorption in this area on the March 10 image. To compensate for these two gradients, we subtracted a linear north-south temperature gradient equivalent to 0.4 C° per 100 km, and a smaller, east-west, second-order power law function from the thermal composite. This removed the large-scale gradients and permitted greater contrast-stretching (without saturation) to better display the eddy-like features in the final version of the composite. The use of such compensating functions in an image with a small number of signal levels would normally introduce "step" features, which would show as slowly curving lines in the image. Although these would not be confused with the smaller-scale eddies discussed here, they are visually distracting artifacts, which we suppressed. This was done by coding fractional increments in pixel signal level as the probability with which that pixel is raised to the next integer level, a technique similar to "stochastic shading". This introduces a small amount of noise in return for considerable cosmetic improvement.

A thermal image for February 28 covered roughly the same region as the image for March 1 and so was not used in the composite; for the two month period prior to February 28, the only other thermal images of the Gulf of Alaska which had useable cloud-free portions were on January 4, 22 and 23 and February 1, 4, 12, 14 and 16 (see Table 1).

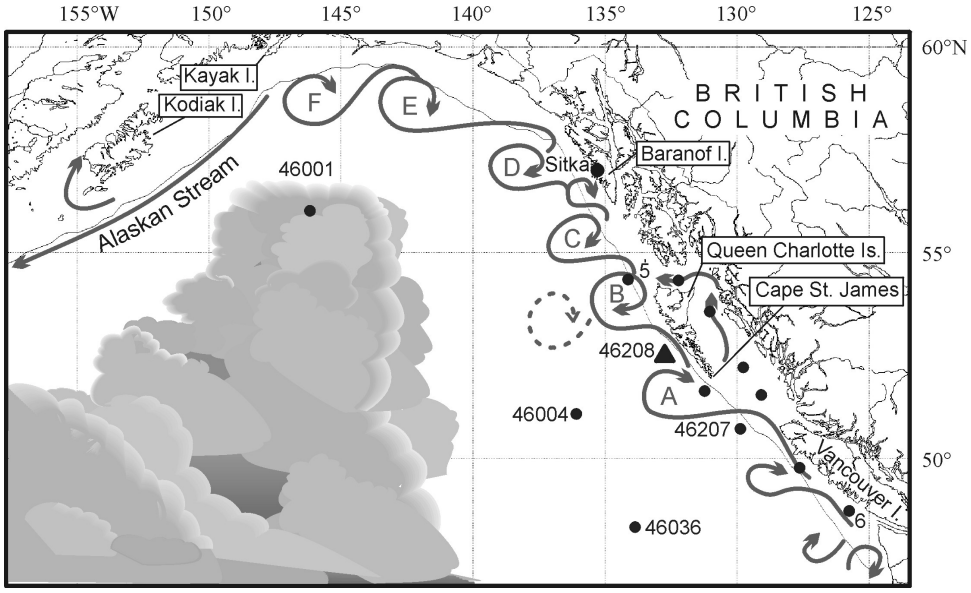

Figure 1.. *The same map of the Gulf of Alaska used in Plate 1 with the authors' interpretation of the current meander pattern suggested by the surface thermal structure. The main eddies are labelled A-F. Two smaller eddies appear off Vancouver Island and northern Washington State (lower right-hand corner of the figure). Dots (•) denote locations of moored meteorological buoys for those referenced in the text (5 = 46205; 6 = 46206); a triangle (▲) is used for meteorological buoy 46208 (see Fig. 3). Dotted line is the 1000 m depth contour.*

3. Mesoscale eddy sequence

The composite satellite image (Plate 1) and our schematic interpretation (Figure 1) of the surface features appearing in the composite image show five, well-defined, equally-spaced oceanic eddies (A-E in Plate 2) strung-out along the coast between central British Columbia and central Alaska. There is a less-well defined sixth eddy (F) to the south of Kayak Island, Alaska, as well as two weaker, more closely spaced, eddies between northern Washington State and northern Vancouver Island. Surface temperatures near the centers of the eddies were 2-3 C° higher than those in the adjoining ocean and inner portion of the shelf. The eddy situated off Sitka, Alaska occurs at the location of the anticyclonic "Sitka eddy" described by *Tabata* (1982). The eddies in the main sequence had a mean radius $r \approx 80 \pm 11$ km ($n = 6$) and were centered over the seaward flank of the continental slope at depths of 2-3 km. For the well-defined eddies in Plate 1, estimates of the eddy center and radius, r, were obtained by fitting two-dimensional top-hat and Gaussian temperature distributions to the observations and seeking those fits that minimized the root-mean-square error between model and observation. [A top-hat model of the azimuthal θ temperature distribution has the form $T_\theta(r) \approx T_o\, h(r_o - r)$ where T_o is a constant, $h(r)$ is the Heaviside step function, and r_o is a scale width for the core of the eddy. For a Gaussian distribution, $h(r)$ is replaced by a function of the form $e^{(-r/r_o)^2}$.] Both fits were significant but we found no statistical justification for choosing one model over the other so results are based on the Gaussian model.

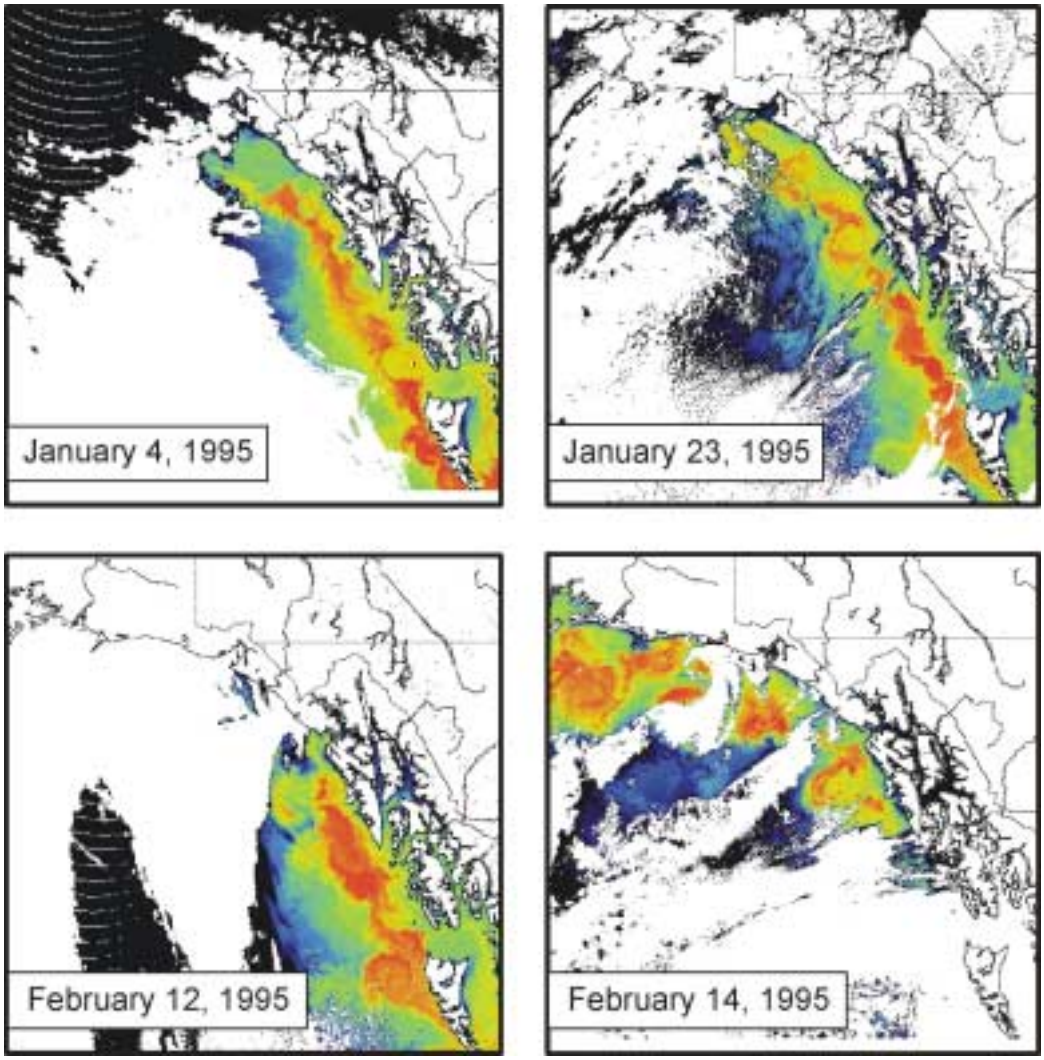

Plate 2. *NOAA AVHRR thermal images for clear areas of the Gulf of Alaska prior to the period of the composite image: (a) January 4, (b) January 23, (c) February 12, and (d) February 14, 1995 (see Table 1 for pass numbers and times).*

Based on the "trailing edge" patterns of kilometer-scale features being shed at the boundaries of the major eddies and the curved paths taken by the relatively low temperature filaments being rolled up (entrained) into the core of the eddies, the flow in all major eddies was clockwise rotary (anticyclonic). The six main eddies had an average alongshore spacing $L_y \approx 247 \pm 33$ km ($n = 5$) while the spacing between the two smaller eddies off Vancouver Island was ~ 150 km. The eddy-like pattern ended immediately to the east (i.e. upstream) of Kodiak Island where the flow narrowed into a comparatively warm, southwestward current centered over the 1000 m isobath. The jet-like structure of the current off Kodiak Island and its confinement to the continental slope suggests that this was the start of the Alaskan Stream [*Thomson*, 1972; *Reed and Stabeno*, 1989].

4. Baroclinic instability of the Coastal Current

Although the oceanic thermal pattern captured by the composite satellite image is quite convoluted, it suggests an underlying spatial continuity of the prevailing flow extending from northern Washington State to Kodiak Island, Alaska (Figure 1). One explanation for the flow pattern, which is consistent with the observed thermal structure and with our present understanding of the regional circulation [*Dodimead et al.*, 1963; *Tabata*, 1975; *Hickey*, 1979; *Strub et al.*, 1987; *Hickey*, 1989; *Smith*, 1995], is that it was associated with a coast-wide instability event in the coastal current regime. The instability mechanism most likely to account for disruption of this flow is baroclinic instability [*Mysak*, 1977; *Pedlosky*, 1978; *Wright*, 1980; *Ikeda et al.*, 1984a,b]. In this process, potential energy stored in the cross-shore gradient, $\partial\overline{\rho}/\partial x$, of the mean density field, $\overline{\rho}$, is transferred to kinetic energy of the eddying motions through non-linear interactions of the form $\overline{\rho u}\,\partial\overline{\rho}/\partial x \propto \overline{\rho u}\,\partial\overline{v}/\partial z$, where ρ and u are perturbations of density and cross-shore velocity, respectively [*Pedlosky*, 1978; *Thomson*, 1984]. The vertical shear, $\partial\overline{v}/\partial z$, in the alongshore component of mean velocity, $\overline{v}$, is related to $\partial\overline{\rho}/\partial x$ through the thermal wind relation given by, $\partial\overline{v}/\partial z = -(g/f\overline{\rho})\,\partial\overline{\rho}/\partial x$ [*Thomson*, 1984], where g is the acceleration of gravity and f is the local Coriolis parameter.

Some form of perturbation in the mean velocity field is needed to trigger the baroclinic instability process, which then evolves from a series of meanders to a series of isolated eddies. Since the transformation from meanders to eddies takes several days to weeks, the instability event must have taken place in sufficient time before March 1, 1995 to allow the initial flow perturbations to amplify into a sequence of mesoscale eddies. Depending on certain physical factors, such as the initial structure of the mean flow and the roughness of the bottom topography, meander growth is dominated by one or two fastest-growing waves with characteristic wavelengths in the range of 50-500 km. Although motions are strongly nonlinear during amplification of the meanders, quasi-geostrophic dynamics dominate the final stages of the process so that the radius, r, of the coastal eddies can be scaled by the internal radius of deformation, $R \equiv NH/f$, where H is the water depth and $N(z) = [-(g/\overline{\rho})\,d\overline{\rho}/dz]^{1/2}$ is the Brunt-Väisälä frequency [e.g., *Thomson*, 1984]. For much of continental slope spanned by the composite thermal image, $H \approx$ 2-3 km, $f \approx 10^{-4}$ s^{-1} and winter values of N range from 10^{-2} s^{-1} at 100 m depth to 10^{-3} s^{-1} at 2500 m depth [*Crawford and Thomson*, 1984; *Thomson and Wilson*, 1987]. Using $N \approx 2\text{-}3 \times 10^{-3}$ s^{-1} as a typical value for water over the outer portion of the continental slope, $R \approx$ 40-90 km, in general agreement with the radius $r \approx 80 \pm 11$ km of the observed eddies. A rule-of-thumb sometimes used to relate the wavelength of the fastest growing wave L_y to the internal deformation radius is $L_y \sim 6R$ [*Wright*, 1980; *Ikeda et*

al., 1984a,b]. This yields $L_y \approx$ 240-540 km, which is marginally consistent with the observed spacing of 247±33 km between eddies.

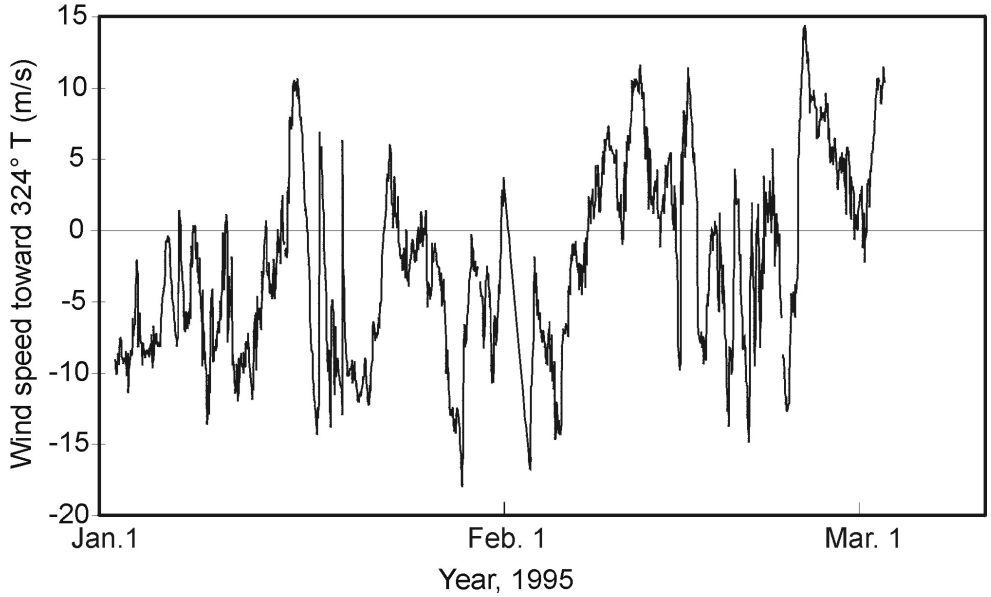

Figure 2. *Time series of the daily-mean alongshore component of wind speed from offshore meteorological buoy 46208 (see Figure 1) for the period January 1 to March 10, 1995. Positive winds blow from the northwest and toward the southeast at 144° True compass bearing. Alongshore winds at site 46208 are similar to those at other coastal locations with typical squared correlation coefficients between sites of ~ 0.78 (e.g., 46208-46205) and 0.69 (e.g., 46208-46207). Winds measured at NOAA weather buoy 46001 in the middle of the Gulf of Alaska (56°N, 148°W) show a major wind reversal in the middle of January similar to that at the coast.*

Coastal baroclinic instability events can be triggered by several mechanisms, including topographic features on the continental slope [*Ikeda et al.*, 1984a,b] and reversals in the local longshore winds [*Thomson and Gower*, 1985]. A possible triggering mechanism for the basin-scale instability event recorded by the composite image was a large-scale reversal in the oceanic winds. Although we cannot rule out the possibility that some of the eddies in the sequence were linked to topographic features [*Tabata*, 1982; *Swaters and Mysak*, 1985] or to local wind reversals, we believe that the most likely triggering event was a coast-wide, two-day duration, wind reversal in mid January (Figure 2). This wind reversal had the spatial extent we think is needed for the basin-scale response of the circulation. Moreover, the time of the wind change is consistent with the absence of mesoscale eddies in an thermal image for January 4 (Plate 2a), and the presence of several mesoscale meanders in the thermal images for late January (Plate 2b), and with the presence of well-developed mesoscale eddies in the images for mid February (Plate 2c and 2d). The relatively small eddy observed to the west of Cape St. James (southern tip of the Queen Charlotte Islands; Figure 1) prior to February 12 is a quasi-permanent feature of the

region which appears to be associated with the outflow of tidally-mixed water from the inner coastal waters [*Thomson and Wilson*, 1987; *Crawford et al.*, 1995].

Between January 14 and 16, winds along the entire coast of the eastern Gulf of Alaska reversed from 10 m s^{-1} downwelling-favorable southeasterlies to 10 m s^{-1} upwelling-favorable northwesterlies. The coastal current would have begun to respond within one inertial period ($T \approx 2\pi / f \approx 16$ hours) to this sudden reversal in the wind stress forcing and, as the northerly winds continued to blow against the opposing current, would have led to increasing vertical shear in the upper ocean currents. This would have been conducive to the onset of baroclinic instability and the growth of mesoscale meanders [*Mysak*, 1977; *Wright*, 1980; *Thomson and Gower*, 1985]. From the positions of the thermal oceanic boundaries in the January to March images (starting with an assumed eddy generation time of January 14), we obtain a mean eddy propagation speed $\bar{c} = 3.0 \pm 0.5$ km d^{-1} (Figure 3), which is consistent with previous estimates of eddy propagation in the northeast Pacific [*Gower*, 1989; *Thomson et al.*, 1989]. Over the 2 day span of the first three images used in the composite (which covers the area where five of the main eddies were present), the eddies would have moved less than 10 km, justifying our assertion that Plate 1 is a true "snapshot" of the surface thermal conditions for the entire coastal region.

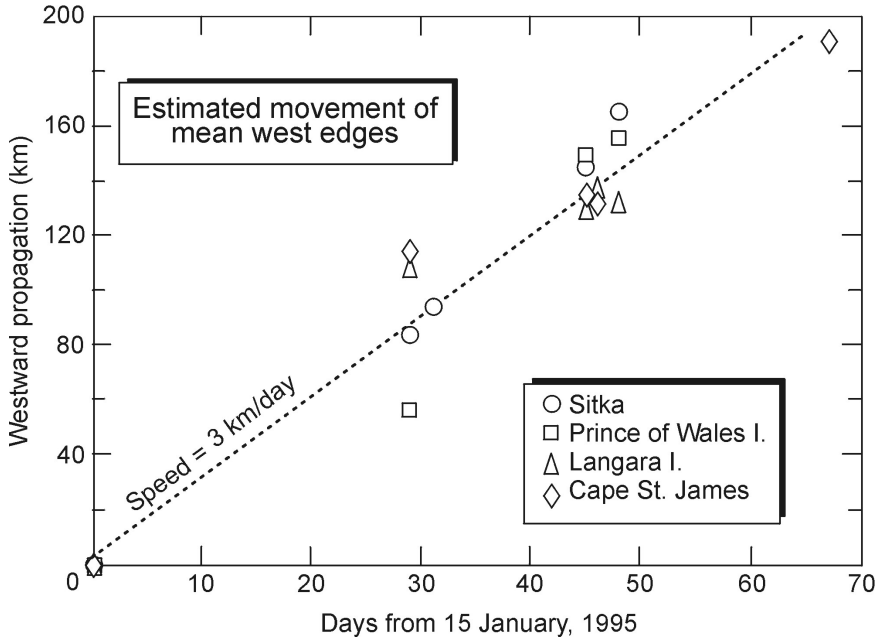

Figure 3. *Estimates of the propagation speeds of the mesoscale eddies based on temporal variations in the seaward boundaries of the eddies for the images of mid February to mid March when the eddies are well developed (Table 1). The edges of the current meanders on January 14 are used as the start times for the calculations.*

We can estimate the growth rates and wavelengths for the fastest-growing waves using the numerical model results of *Ikeda et al.* (1984a, b) for the west coast of Vancouver Island at the southern end of the study region. Building on a two-layer model for the region by *Mysak* [1977] and three-layer models for the region by *Wright* [1980] and *Ikeda* [1983], *Ikeda et al.* [1984a] assume a four-layer model for the density and alongshore current, with a vertical 2000 m deep eastern boundary and a gently sloping seafloor. Modeled winter currents consist of equally strong ≈ 20 cm s^{-1} poleward flows in the upper two layers (corresponding to a 150 m thick surface current and a 450 m thick California Undercurrent) and zero flow in the two bottom layers. The zero mean flow in the two bottom layers and the small density difference between these layers is intended to model the weak outer slope currents observed in current meter records for the region. Although the model is not strictly applicable to the deeper (> 2500 m) continental margin to the north of Vancouver Island (where we found the most distinct eddies), results for winter flow are in agreement with our observations of short (150 km) spacing between the two weak eddies off the island (Plate 1 and Figure 1). For initially poleward flow in the two upper layers, the fastest-growing wavelengths in the model were ~ 150 km, with e-folding time scales of 10-15 days and alongshore propagation speeds of 2-3 cm s^{-1} (1.7 to 2.6 km d^{-1}). This wavelength is considerably less than the ~250 km wavelength of the six main eddies in the composite image (Plate 1). However, as noted by *Ikeda et al.* [1984a], as the vertical shear between the top two layers is reduced (as would be the case immediately following the wind reversal), the baroclinic instability due to the shear between the undercurrent and the lower ocean becomes more important. The fastest growing surface waves would have smaller growth rates and longer wavelengths than for the case of surface-dominated shear. This effect, combined with the greater water depth (hence, greater horizontal scale, NH/f), might account for the relatively slow growth and large spacing of the eddy sequence observed off northern British Columbia and central Alaska in early 1995.

4. Summary and Conclusions

Our analysis suggests that the poleward current that forms along the northwest continental margin of North America in late fall (which we have tentatively called the Northeast Pacific Coastal Current) is a simply connected flow regime that can undergo basin-scale baroclinic instability triggered by large-scale reversals in the prevailing cyclonic winds. The current deforms into a series of mesoscale eddies which then detach from the coast and propagate slowly westward into the ocean. Provided the event occurs early enough in the season that winds again blow cyclonically around the basin, the coastal current could reform and the process begin again.

Regardless of the mechanism generating the instability event in the coastal current, there is little doubt that the event had a major impact on the circulation and water property distribution along the eastern Gulf of Alaska. As indicated by Plate 1, the influence of the instability was not limited to the continental slope but

extended well onto the shelf and into the offshore region. Specifically, the breakup of the current into a series of persistent mesoscale eddies would have increased the effective horizontal turbulent eddy diffusion, ν_H, and hence the transport of entrained coastal water into the open ocean. Prior to the event, we expect a relatively low eddy diffusion $\nu_H \propto \langle uv \rangle LU^{-1} \approx 10^3\ \mathrm{m^2 s^{-1}}$ based on simple scaling arguments for small-scale horizontal turbulent motions $u, v \approx 0.1\ \mathrm{m\,s^{-1}}$, and an assumed mean flow $U \approx 1\ \mathrm{m\,s^{-1}}$ spanning a cross-shore scale $L \approx 100$ km ($\langle\rangle$ denotes an ensemble average). Following formation of the eddies, the turbulent motions would have increased in speed and become more spatially coherent, significantly increasing the Reynolds stress, $\langle uv \rangle$. If we assume that the eddies had characteristic current speeds $u, v \approx 0.5\ \mathrm{m\,s^{-1}}$ but retain the same pre-event scales *U* and *L*, we find $\nu_H \approx 10^4\ \mathrm{m^2 s^{-1}}$, which suggests at least an order of magnitude increase in the eddy-induced transport of brackish coastal water into the Gulf of Alaska.

Few suitably cloud-free periods occur in the northeast Pacific to generate composite images of the extent of Plate 1. Cloud-coverage is also the reason we could not determine the fate of the March 1995 eddies as they moved offshore. Nevertheless, we found sufficient numbers of satellite images in our data archive to indicate that basin-scale instability events similar to that for January-March 1995 may not be rare. The earliest evidence we could find for such an event was a low-quality NOAA 5 thermal image for January 3, 1978 which shows a sequence of four mesoscale coastal eddies extending over 600 km from the southern end of the Queen Charlotte Islands to the northern end of the Alaskan Panhandle. Three eddy-like features appear in the northward flowing Haida Current off the Queen Charlotte Islands in the NOAA thermal image for January 22, 1983 [*Thomson and Emery*, 1986] and four mesoscale eddies originating at widely separated locations along the coast in February 1987 were tracked across the Gulf of Alaska by *Gower and Tabata* [1996] using the 17-day repeat orbit data from the GEOSAT Altimeter. The occurrence of a further two eddies in the same region in February 1988 points to an annual cycle of eddy generation [*Gower and Tabata*, 1996]. We further remark that winds from the coastal meteorological buoys (see Figure 1) reveal a large-scale wind reversal in the Gulf of Alaska around the end of December 1994, a month or so before the mid-January event reported here. Again, coastal winds at the time reversed from strong southeasterlies to strong northwesterlies. The faint eddy-like feature seaward of the northwest tip of the Queen Charlotte Islands (the dashed curve in Plate 1) may be the remnant of an earlier eddy formed during a local wind event or other instability process.

If the instability events were to occur once or twice each winter (specifically, late fall to early spring), they could be an important mechanism for the coast-wide flushing of brackish, nutrient-rich surface water into the Gulf of Alaska. Biological activity in the coastal waters might be disrupted for many weeks during each instability event and passively drifting organisms, such as eggs and larvae on the shelf and slope, could be

transported seaward and dispersed. The timing of the instability events with respect to the annual growth and reproductive stages of fish and zooplankton stocks over the continental margin would be critical [e.g., *MacFarlane et al*., 1997]. The organisms also might be retained for long periods in eddies shed from the coast. In this regard, we note that satellite-tracked surface drifters deployed in the northeast Pacific over the past several decades [e.g., *Thomson et al.*, 1990] often become trapped in persistent (up to 10 months), westward-propagating (~1 km d^{-1}) mesoscale eddies of possible coastal origin. Additional observations, combined with numerical modeling of the instability events, would aid in our understanding of this important dispersion mechanism and associated circulation in the Gulf of Alaska.

Acknowledgments. We thank Robert Shanks and John Wallace for helping generate the composite image, Patricia Kimber for assisting with the figures, and Robin Brown and Josef Cherniawsky for working up the wind data. We thank the reviewers for their helpful comments, especially for suggesting that we expand our work to include a conceptual model for the Gulf of Alaska circulation.

References

Crawford, W.R. and R.E. Thomson, Diurnal-period continental shelf waves along Vancouver Island: A comparison of observations with theoretical models, *J. Phys. Oceanogr*., *14*, 1629-1646, 1984.

Crawford, W.R., M.J. Woodward, M.G.G. Foreman, and R.E. Thomson, Oceanographic features of Hecate Strait and Queen Charlotte Sound in summer, *Atmosphere-Ocean, 33*, 639-681, 1995.

Dodimead, A.J., F. Favorite, and T. Hirano, Salmon of the North Pacific Ocean-Part II. Review of oceanography of the subarctic Pacific region, *Int. North Pac. Salmon Commission Bull*., *13*, 195 p., 1963.

Gower, J.F.R., Geosat altimeter observations of the distribution and movement of sea-surface height anomalies in the north-east Pacific, in *The Global Ocean*, pp. 977-981, Oceans ‘89, September 18-21, 1989, Seattle Wash., Vol. 3, IEEE Publ. No. 89CH2780-5, 1989.

Gower, J.F.R. and S. Tabata, Measurements of eddy structure and movement in the North-East Pacific with the GEOSAT altimeter, in *PORSEC-’92 Proceedings Vol. 2.*, pp. 614-621, 1992.

Hickey, B.M., The California Current system - hypotheses and facts, *Prog. in Oceanogr*., *8*, 191-279, 1979.

Hickey, B.M., Patterns and processes of circulation over the Washington continental shelf and slope, in *Oceanography of the Washington-Oregon Coastal Zone*, edited by M. Landry and B. Hickey, pp. 41-109, Elsevier, Amsterdam, 1989.

Ikeda, M., Linear instability of a current flowing along a bottom slope using a three-layer model, *J. Phys. Oceanogr*., *13*, 208-223, 1983.

Ikeda, M., L.A. Mysak, and W.J. Emery, Observations and modeling of satellite-sensed meanders and eddies off Vancouver Island, *J. Phys. Oceanogr*., *14*, 3-21, 1984a.

Ikeda M., L.A. Mysak, and W.J. Emery, Seasonal variability in meanders of the California Current system off Vancouver Island, *J. Geophys. Res*., *89*, 3487-3505, 1984b.

LeBlond, P.H., K. Dyck, K. Perry, and D. Cumming, Runoff and precipitation time series for the coasts of British Columbia and Washington State, *Dept. Oceanogr., Univ. B.C.*, No. 39, 133 pp., 1983.

LeBlond, P.H., B.M. Hickey, and R.E. Thomson, Runoff driven coastal flow off British Columbia, in *The role of freshwater outflow in coastal marine ecosystems*, edited by S. Skreslet, pp. 309-317, NATO ASI Series, Vol. G7, Springer-Verlag, Berlin, 1986.

Marmer, H.A., Coastal currents along the Pacific coast of the United States, *U.S. Coast Geod. Survey Spec. Publ*., *121*, 80 pp., 1926.

McFarlane, G.A., D.M. Ware, R.E. Thomson, D.L. Mackas, and C.L.K. Robinson, Physical, biological and fisheries oceanography of a large ecosystem (west coast of Vancouver Island) and implications for management, *Oceanologica Acta*, *20*, 191-200, 1997.

Mysak, L.A., On the stability of the California Undercurrent off Vancouver Island, *J. Phys. Oceanogr*.,*7*, 904-917, 1977.

Pedlosky, J., *Geophysical Fluid Dynamics*, 624 pp., Springer-Verlag, New York, 1978.

Reed, R.K. and P.J. Stabeno, Recent observations of variability in the path and vertical structure of the Alaskan Stream, *J. Phys. Oceanogr*., *19*, 1634-1642, 1989.

Royer. T.C., Baroclinic transport in the Gulf of Alaska. Part II. A fresh water driven coastal current, *J. Mar. Res*., 39, 251-266, 1981.

Smith, R.L., The Physical Processes of Coastal Ocean Upwelling Systems, in *Upwelling in the Ocean: Modern Processes and Ancient Records*, edited by C.P. Summerhayes, K.-C. Emeis, M.V. Angel, R.L. Smith, and B. Zeitzschel, pp. 39-64, John Wiley & Sons Ltd., New York.

Strub, P.T., J.S. Allen, A. Huyer, R.L. Smith, and R.C. Beardsely, Seasonal cycles of currents, temperatures, winds, and sea level over the northeast Pacific continental shelf: 35°N to 48°N, *J. Geophys. Res*., *92*, 1507-1526, 1987.

Swaters, G.E., and L.A. Mysak, Topographically-induced baroclinic eddies near a coastline, with application to the Northeast Pacific, *J. Phys. Oceanogr.*, *15*, 1470-1485, 1985.

Tabata, S., The general circulation of the Pacific Ocean and a brief account of the oceanographic structure of the North Pacific Ocean, *Atmosphere*, *13*, 133-168, 1975.

Tabata, S., The anticyclonic, baroclinic eddy off Sitka, Alaska, in the Northeast Pacific Ocean, *J. Phys. Oceanogr.*, *12*, 1260-1282, 1982.

Thomson, R.E., On the Alaskan Stream, *J. Phys. Oceanogr.*, *2*, 363-371, 1972.

Thomson, R.E., A cyclonic eddy over the continental margin of Vancouver Island: Evidence for baroclinic instability, *J. Phys. Oceanogr. 14*, 1326-1348, 1984.

Thomson, R.E. and J.F. Gower, A wind-induced mesoscale eddy over the Vancouver Island continental slope, *J. Geophys. Res*., *90*, 8981-8993, 1985.

Thomson, R.E. and W.J. Emery, The Haida Current, *J. Geophys. Res*., *91*, 845-861, 1986.

Thomson, R.E. and R.E. Wilson, Coastal counter-current and mesoscale eddy formation by tidal rectification near and oceanic cape, *J. Phys. Oceanogr*., *11*, 2096-2126, 1987.

Thomson, R.E. and W.J. Emery, The Haida Current, *J. Geophys. Res*., *91*, 845-861, 1986.

Thomson, R.E., B.M. Hickey, and P.H. LeBlond, The Vancouver Island Coastal Current: Fisheries barrier and Conduit, in *Effects of ocean variability on recruitment and an evaluation of parameters used in stock assessment models*, edited by R. Beamish and G. McFarlane, pp. 265-296, *Can. Spec. Publ. Fish. Aquatic Sci. 108*, Ottawa, 1989.

Thomson, R.E., P. H. LeBlond, and W.J. Emery, Analysis of deep-drogued satellite-tracked drifter measurements in the northeast Pacific, *Atmosphere-Ocean*, *28*, 409-443, 1990.

Thomson, R.E. and D.M. Ware, A current velocity index of ocean variability, *J. Geophys. Res*., *101*, 14,297-14,310, 1996.

Wright, D.G., On the stability of a fluid with specialized density stratification, 2, Mixed baroclinic-barotropic instability with application to the northeast Pacific, *J. Phys. Oceanogr.*, *10*, 1307-1322, 1980.